ACS APPLIED MATERIALS & INTERFACES

Research Article

www.acsami.org

Facile Green In Situ Synthesis of Mg/CuO Core/Shell Nanoenergetic Arrays with a Superior Heat-Release Property and Long-Term Storage Stability

Xiang Zhou, Daguo Xu, Qiaobao Zhang, Jian Lu, and Kaili Zhang*

Department of Mechanical and Biomedical Engineering, City University of Hong Kong, 83 Tat Chee Avenue, Kowloon, Hong Kong

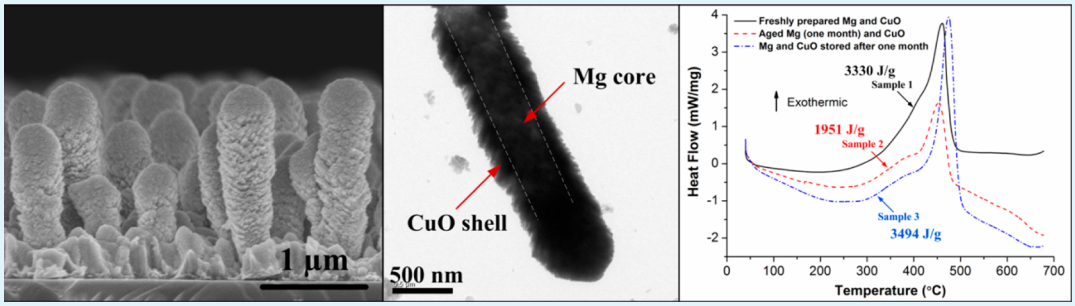

ABSTRACT: We report a facile green method for the in situ synthesis of Mg/CuO core/shell nanoenergetic arrays on silicon, with Mg nanorods as the core and CuO as the shell. Mg nanorods are first prepared by glancing angle deposition. CuO is then deposited around the Mg nanorods by reactive magnetron sputtering to realize the core/shell structure. Various characterization techniques are used to investigate the prepared Mg/CuO core/shell nanoenergetic arrays, including scanning electron microscopy, transmission electron microscopy, X-ray energy dispersive spectroscopy, X-ray diffraction, and thermal analysis. Uniform mixing and intimate contact between the Mg nanorods and CuO are confirmed from both visual inspection of the morphological images and analyses of the heat-release curves. The nanoenergetic arrays exhibit a low-onset reaction temperature (~300 °C) and high heat of reaction (~3400 J/g). Most importantly, the nanoenergetic arrays possess long-term storage stability resulting from the stable CuO shell. This study provides a potential general strategy for the synthesis of various Mg nanorod-based stable nanoenergetic arrays.

KEYWORDS: *Mg/CuO core/shell, nanoenergetic arrays, facile green in situ synthesis, long-term storage stability, high heat of reaction*

1. INTRODUCTION

Nanoenergetic materials (nEMs) have received continuously increasing interest because of their unique combustion velocity,[1−3] ignition/onset-reaction temperature,[4,5] ignition delay,[6] and apparent activation energy[7] properties compared to those of traditional energetic materials (propellants, explosives, and pyrotechnics), leading to diverse promising applications in both the civilian and military fields such as airbags, belt tensioners, mining, deconstruction, heat sources for rapid fuses, the joining of materials by means of localized heating, micropropulsion systems, percussion or electric primers, explosive additives, propellant rate modifiers, arms fire, and safety and arming devices used in missiles/rockets.[8−11] Many methods have been used to synthesize nEMs, with powder mixing,[1,3] sol−gel,[12,13] layered vapor deposition,[5,14] arrested reactive milling,[15,16] and porous silicon with an embedded oxidizer[8,17] being the most frequently employed. Besides their respective merits, these methods suffer from certain drawbacks, such as inherent impurities, nonintimate contact, and nonhomogeneous distribution of oxidizer and fuel, leading to a large scatter in their ignition and burning characteristics.[18] The nEMs synthesized by many of the aforementioned methods are not suitable for integration with microelectromechanical systems (MEMS) to realize functional nanoenergetics-on-a-chip, which is one key to a great advance in microscale energy-demanding devices such as those used in microactuation, microignition, micropropulsion, and micropower.[19]

Recently, core/shell structured CuO/Al nEMs have been synthesized by integrating nano Al (by thermal evaporation or sputtering) with 1D CuO nanowires grown from Cu films/foils,[20] with CuO nanowires as the core and Al as the shell.[21−24] This synthesis strategy has the advantages of improved mixing uniformity, enhanced contact, reduced impurities, and lower activation energy. Nevertheless, the nanostructure (CuO nanowires) is only a very small portion of the entire structure, whereas a big portion of the structure is in the form of the microscale film that lays underneath the CuO nanowires (Figure 1a). The Al is not contacting much of the film, which significantly affects the heat-release property of the nEMs.[21,24] A similar problem also exists for the CuO/Al core/shell nEMs.[22] There is a 2 μm thick CuO film layer beneath the CuO

Received: May 22, 2013
Accepted: July 19, 2013
Published: July 19, 2013

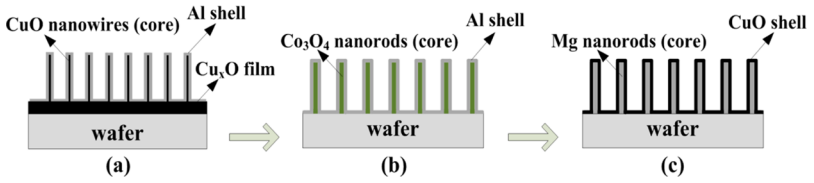

Figure 1. Schematics of three kinds of core/shell nanoenergetic arrays on a substrate. (a) First generation with the existence of a microscale oxide film,[21−24] (b) pure core/shell nanostructure (no microstructure) with oxide as the core and metal as the shell,[25] and (c) new concept of a pure core/shell nanostructure with metal as the core and stable oxide as the shell (the present work).

nanowires. The CuO film layer was found to react with Al at a higher temperature compared to that of CuO nanowires, which leads to the broadening of the heat-release profile. It is desirable to have nEMs composed of pure nano fuel and oxidizer (no microscale fuel and oxidizer exist), which are expected to demonstrate improved performance. For instance, nanostructures (CuO nanowires) have been proven to enhance the exothermic reactions and reduce the ignition delay and ignition energy of CuO/Al nEMs.[23] In 2012, Xu et al. used a chemical method to synthesize pure Co_3O_4 nanorods (no microscale film) and then deposit nano Al around the Co_3O_4 nanorods to realize core/shell nanoenergetic arrays (Figure 1b).[25] The prepared Co_3O_4/Al was confirmed to have very high heat of reaction and significantly reduced onset reaction temperature.

However, in the previous core/shell structure-based approaches,[21−25] metal-oxide (CuO and Co_3O_4) nanowires/rods are first synthesized followed by nano Al integration around the nanowires/rods to achieve the core/shell nEMs with metal-oxide as the core. As a result, active nano Al is exposed to the environment (e.g., moisture in the air) as the shell (Figures 1a,b). This will cause the oxidation of Al, resulting in a degraded performance of the nEMs, especially if the nEMs need to be stored for long-term use. It has been found that nano Al is readily oxidized during long-term storage.[26] Therefore, it is beneficial if we first synthesize fuel (e.g., Al and Mg) nanowires/rods and then integrate metal-oxidizer around them to achieve core/shell-based nEMs with fuel as the core and metal-oxide as the shell. The stable metal-oxide shell will make the realized nEMs more resistant to the environment. Moreover, almost all of the previous procedures adopted to realize core/shell nEMs involve high temperature[21−25] and/or chemical solution,[25] which is energy consuming, not green, and can restrict further the compatibility with other processing steps when considering integration with MEMS to achieve functional devices.

In this study, Mg nanorod arrays are first deposited on silicon substrates by glancing angle deposition followed by CuO integration around the Mg nanorods by reactive magnetron sputtering to achieve Mg/CuO core/shell nanoenergetic arrays, with Mg as the core and CuO as the shell. The stable CuO shell will make the realized nEMs more resistant to the environment. Furthermore, the whole process is facile, green, and the temperature of the substrate/nEMs is very low (<80 °C) during synthesis. The schematic of our new concept is shown in Figure 1c.

2. EXPERIMENTAL SECTION

Half of a 4 in. single-crystal silicon wafer is cleaned in acetone with ultrasonic vibration. It is then thoroughly rinsed by deionized water and blown dry by compressed air. Mg nanorods are fabricated onto the silicon substrate by the glancing angle thermal deposition of 99.95% pure Mg pellets (Alfa Aesar, 0.125″ diameter × 0.25″ length), with a tungsten boat as the heater in a conventional thermal evaporator (Denton DV502A). The incident angle of the Mg vapor flux with respect to the substrate surface normal is fixed at 84°. The average distance between the substrate and Mg source is about 8 cm. After the vacuum level in the evaporator chamber reaches 2×10^{-6} Torr, the evaporation starts with a constant current of about 2.5 A, and the deposition rate on a flat surface is 10−15 Å/s. The temperature of the substrate is determined to be below 80 °C during the deposition process. CuO is then deposited to surround the as-prepared Mg nanorods by reactive magnetron sputtering with oxygen as the reactive gas and copper as the target (Kurt J. Lesker, 3.0″ diameter × 0.125″ thickness, 99.99% purity), and argon gas is used as the working atmosphere. The flow rates of Ar and O_2 are kept as 100 and 20 sccm, respectively, and the sputtering power is 60 W. The base vacuum and working pressure are 1×10^{-6} and 6.5×10^{-4} Torr, respectively, and the deposition rate of CuO on a flat surface is about 20 nm/min. The as-synthesized Mg nanorods and Mg/CuO nanoenergetic arrays are directly observed with a field emission scanning electron microscope (Hitachi S4800 FESEM). X-ray diffraction (Rigaku SmartLab XRD) is used to determine the compositions of the as-prepared Mg/CuO nanoenergetic arrays as well as the corresponding reaction products after thermal analysis. The freshly prepared Mg nanorods and Mg nanorods stored in a dry cabinet for 1 month are characterized with an energy dispersive spectrometer (Oxford Instruments/INCA Energy 200 EDS) to compare the relative content variations between Mg and O. Transmission electron microscope (FEI Tecnai G2 20 TEM) is also used to check the aged Mg nanorods and the Mg/CuO core/shell structure in which the Mg nanorods are freshly prepared. To prove the long-term storage stability of our new nanoenergetic arrays, three kinds of samples are prepared and compared by differential scanning calorimetry (TA Instruments Q20 DSC). For sample 1, CuO is deposited around freshly prepared Mg nanorods and DSC analysis is performed instantly. For sample 2, Mg nanorods are first stored in a dry cabinet for 1 month before integration with CuO. For sample 3, CuO is deposited around freshly prepared Mg nanorods and the Mg/CuO nanoenergetic arrays are kept in a dry cabinet for 1 month before DSC characterization. Freshly prepared Mg/CuO is also characterized by differential thermal/thermo-gravimetric analysis (TA Instruments Q600 DTA-TG). Samples are scraped from the silicon substrate with a sharp blade, and platinum crucibles are used for both DSC and DTA-TG tests. DSC analyses are performed from 40 to 680 °C with a heating rate of 5 °C/min under 75 mL/min Ar flow, and the masses of the three samples are 4.2, 2.47, and 2.39 mg, respectively. The DTA-TG test is conducted from 40 to 800 °C with a heating rate of 10 °C/min under 100 mL/min Ar flow, and the mass of the sample is 6.78 mg. To remove the oxygen that could possibly be absorbed by the samples as well as to obtain a stable Ar atmosphere during thermal testing, the Ar flow is started 10 min before increasing the temperature.

3. RESULTS AND DISCUSSION

3.1. SEM and EDS Characterization. Figure 2 shows the SEM images of Mg nanorods and Mg/CuO nanoenergetic arrays. Figure 2a,d shows the top-view images of Mg nanorods and Mg/CuO, respectively. Figure 2b,e shows the cross-sectional views of Mg nanorods and Mg/CuO, respectively, from the direction parallel to the Mg vapor flux. Figure 2c,f shows the cross-sectional images from the direction normal to

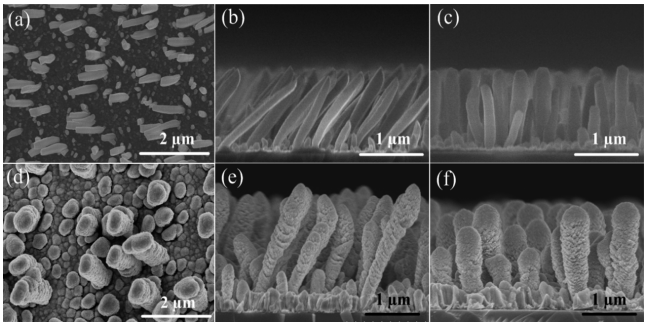

Figure 2. SEM images of (a–c) Mg nanorods and (d–f) Mg/CuO nanoenergetic arrays. (a, d) Top-view images, (b, e) cross-sectional images from the direction parallel to the Mg vapor flux, and (c, f) cross-sectional images from the direction vertical to the Mg vapor flux.

the Mg vapor flux. The growth of the Mg nanorods by glancing angle deposition is widely accepted to be dominated by atomic shadowing and adatom diffusion mechanisms.[27,28] As can be seen from Figure 2a–c, Mg nanorods with diameters of about 150–200 nm have been synthesized on the silicon substrate, and the nanorods exhibit an almost equal diameter from the base to the top.

The deposition rate of CuO on the Mg nanorods is different from that on a flat surface like silicon, and it is difficult to determine the rate accurately. Therefore, in this work, nominal thickness is used to describe the theoretic thickness of CuO according to the deposition rate on a flat silicon surface. After deposition of nominal 500 nm thick CuO by sputtering, the as-prepared Mg/CuO nanoenergetic arrays show increased diameter and length, as shown in Figure 2d–f. Because of the high kinetic energies of the ejected particles in the magnetron sputtering process, CuO can reach the base of the Mg nanorods, which ensures a good quality coating effect. However, it is still found that the diameter of the Mg/CuO decreases slightly from the top to the base.

Figure 3 shows the EDS characterizations of freshly prepared Mg nanorods as well as the Mg nanorods stored in a dry cabinet for 1 month. As can be seen from Figure 3a, there is a small amount of oxygen in the freshly prepared Mg nanorods, which is due to the inevitable oxidation of the highly reactive Mg nanorods that occurs when they are taken out of the vacuum chamber. The strong silicon signal in Figure 3a originates from the silicon substrate. Figure 3b shows the aged Mg nanorods after 1 month storage. It can be clearly seen that the relative content of O versus Mg increases significantly, and the carbon signal can derive from the adsorbed carbon on the surface of the Mg nanorods during storage. From the weight percentage data, we calculate that the atomic ratio of Mg versus O changes from 7.6 to 1.1, and the atomic ratio of 1.1 approaches the stoichiometric value of MgO, which means that the surface of the aged Mg nanorods is almost totally oxidized to MgO. Although EDS characterization is not accurate enough for a precise quantitative analysis, especially for some light elements, it is still quite useful for semiquantitative comparisons. Metallic (e.g., Mg) nanostructures are easily oxidized even in a dry atmospheric environment. Therefore, the long-term storage problem should be taken seriously.

3.2. TEM Characterization. Figure 4a,b and c,d show the bright-field TEM images and the corresponding selected area electron diffraction (SAED) figures of the aged Mg nanorods stored in a dry cabinet for 1 month and the freshly prepared

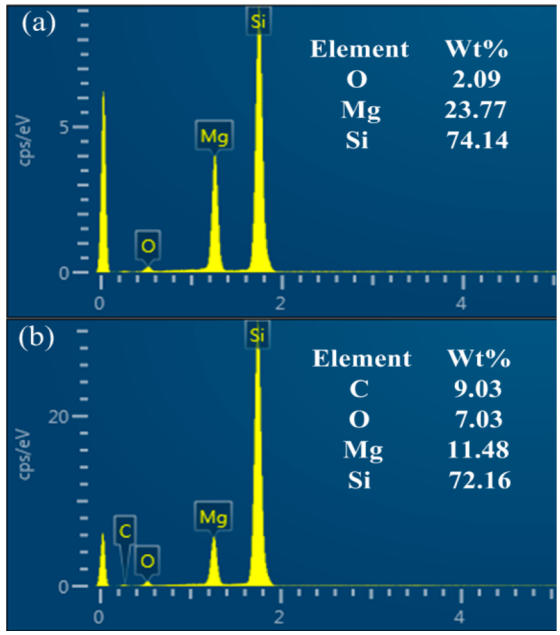

Figure 3. EDS characterizations of Mg nanorods. (a) Freshly prepared Mg nanorods and (b) Mg nanorods stored for 1 month.

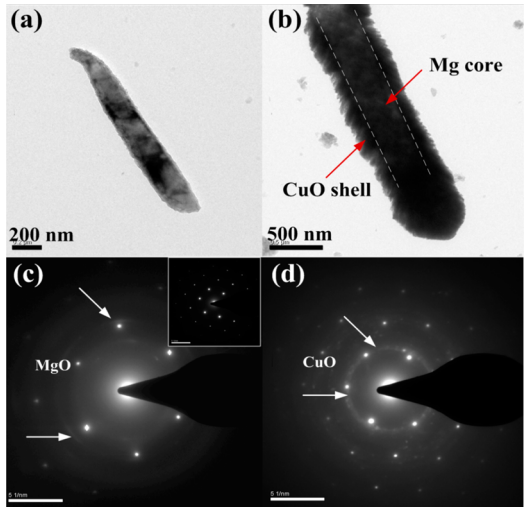

Figure 4. Bright-field TEM images and the corresponding SAED patterns of (a, c) the aged Mg nanorods stored in a dry cabinet for 1 month (the inset of Figure 4c is the electron diffraction pattern of the freshly prepared Mg nanorods) and (b, d) the freshly prepared Mg/CuO core/shell structure.

Mg/CuO nanoenergetic arrays, respectively. Figure 4c,d indicates the single-crystal nature of the whole Mg nanorod, with a hexagonal compact structure, which is identical to the result reported before.[27] Compared with the well-defined dotted pattern of the freshly prepared Mg nanorods (inset of Figure 4c), the dotted pattern becomes vague for the aged Mg nanorods and there are some circles appearing, as indicated in Figure 4c, which are identified as polycrystalline MgO. This means that the Mg nanorods have been partly oxidized to MgO after 1 month of storage, which corresponds well to the EDS results. The Mg/CuO core/shell structure can be seen clearly in Figure 4b, and the polycrystalline CuO shell is composed of many columns similar to that shown in the SEM images in Figure 2d–f. The detailed crystal growth and crystal structures

dx.doi.org/10.1021/am401955u | ACS Appl. Mater. Interfaces 2013, 5, 7641–7646

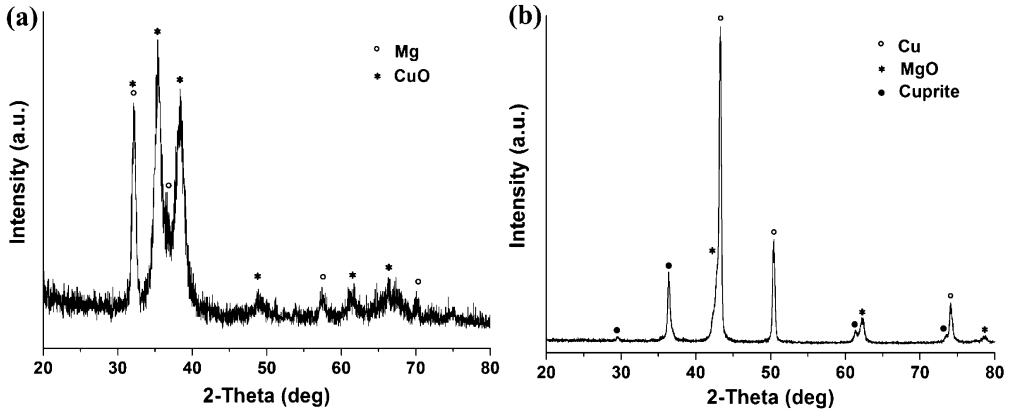

Figure 5. XRD patterns. (a) As-prepared Mg/CuO and (b) reaction products after the DTA-TG test.

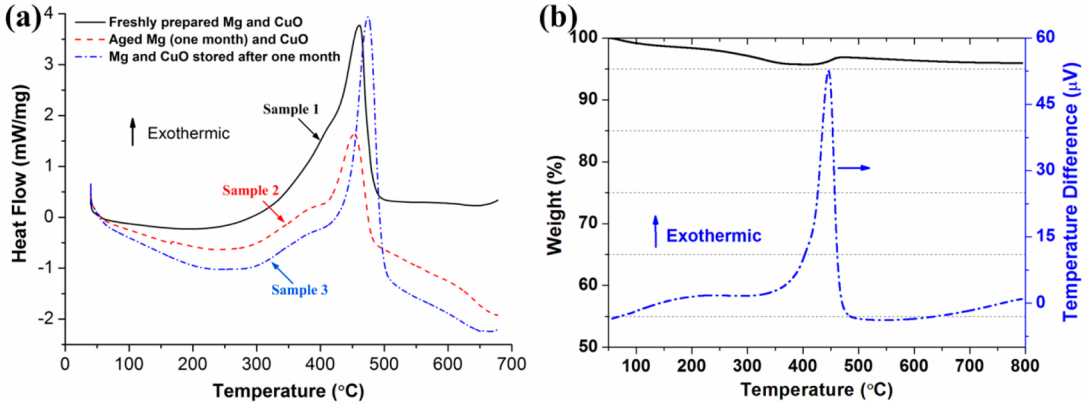

Figure 6. Thermal analysis results. (a) DSC characterizations for three kinds of Mg/CuO nanoenergetic arrays and (b) DTA-TG analysis of freshly prepared Mg/CuO nanoenergetic arrays.

of the MgO and CuO shells are not the focus of this study, so a further analysis of the TEM result is not provided here.

3.3. XRD Characterization. Figure 5 shows the XRD results for the freshly prepared Mg/CuO nanoenergetic arrays as well as the corresponding reaction products collected after the DTA-TG test. As can be seen from Figure 5a, only characteristic peaks of metallic Mg and CuO are found, indicating no obvious prereaction between the Mg nanorods and oxygen during the reactive magnetron sputtering deposition of CuO. The XRD pattern of aged Mg nanorods after 1 month storage in a dry cabinet (data not shown) shows no peaks for MgO as well. The Mg nanorods are proven to be partly oxidized in the EDS and TEM figures, but the naturally formed MgO is not well crystallized and/or it can be nanocrystalline. Consequently, XRD cannot detect it. Figure 5b shows the XRD pattern of the thermite reaction products of the Mg/CuO nanoenergetic arrays after the DTA-TG test. Cu and MgO are clearly seen as reaction products in accordance with the chemical reaction in eq 1. There are also some peaks appearing that are indexed to cuprite, which could be formed by the reaction between excessive reactant CuO and product Cu.

$$\mathrm{Mg} + \mathrm{CuO} \rightarrow \mathrm{MgO} + \mathrm{Cu};$$
$$\Delta H = 4610\ \mathrm{J/g},\ T_{ad} = 2843\ \mathrm{K} \quad (1)$$

where ΔH denotes the heat of reaction and T_{ad} is the adiabatic reaction temperature.

3.4. Thermal Analysis. According to our preliminary tests, CuO with a nominal 500 nm thickness is too much to achieve an ideal equivalent ratio with the Mg nanorods. Therefore, samples used for the DSC and DTA-TG tests are prepared by sputtering nominal 200 nm thick CuO around the Mg nanorods. The DSC results of three kinds of samples are shown in Figure 6a, and Figure 6b exhibits the DTA-TG characterization results for the freshly prepared Mg/CuO nanoenergetic arrays. Three plots in Figure 6a show similar trends but different values. TA Instruments Universal Analysis 2000 software is used to determine the onset reaction temperature and the heat of reaction. The onset reaction temperatures of freshly prepared Mg/CuO (sample 1), Mg aged for 1 month and CuO (sample 2), and Mg/CuO stored for 1 month (sample 3) are 307, 276, and 302 °C, respectively. Samples 1 and 3 show very similar onset reaction temperatures. However, it is unexpected that sample 2 exhibits even lower onset reaction temperature because it was speculated that the naturally formed MgO layer in sample 2 would hinder the initiation of the thermite reaction, causing a higher onset reaction temperature.

We suggest two reasons for this unexpected phenomenon. The first is that the CuO layer is deposited by reactive magnetron sputtering with a copper target and oxygen atmosphere. Therefore, during the sputtering process, especially at the beginning of the deposition, it is likely that there will be some Mg that gets oxidized to MgO. Actually, the oxidation of Al to Al_2O_3 in a similar process has been reported before.[5] Consequently, an MgO layer will also form between

the Mg nanorods and CuO for samples 1 and 3. However, this layer should be very thin because it cannot be detected by XRD. Additionally, the thin MgO layer does not significantly affect the amount of heat released (indicated from the discussion that follows). However, because a naturally formed relatively thick MgO layer already exists around the Mg nanorods in sample 2, it will effectively restrict the generation of more MgO during the reactive sputtering process. The second reason is that the characteristics of the MgO generated during the reactive sputtering process should be different from those of the MgO formed from natural oxidation because high-energy plasma and a relatively higher temperature are involved in the sputtering process. Consequently, although the thickness of MgO layers in samples 1 and 3 could be smaller than that of sample 2, the characteristics of the MgO layer formed during sputtering may play a dominant role in the initiation of the thermite reaction instead of the thickness, leading to a slightly higher onset reaction temperature in samples 1 and 3. In one recently published paper,[29] it was revealed that it is the nature of the monolayer interface between the CuO and alumina/Al rather than the thickness of the alumina layer that controls the kinetics of Al diffusion. Over all, the three samples exhibit very low onset reaction temperatures, which can be attributed to the nanoscale intimate contact between the fuel Mg and the oxidizer CuO and can be beneficial for reducing ignition delay and ignition energy. The DTA curve in Figure 6b shows only one exothermic peak and no melting endothermic peak, which are in accordance with the DSC results. The TG curve shows a gradual decrease at first and then levels off. It is known that CuO is hydrophilic. When scraping the Mg/CuO from the substrate to prepare the sample for thermal analysis, CuO will easily absorb moisture from the air. The humidity of the air during the period of this work is very high, and the initial 4% loss in weight can be due to the desorption of moisture.

The heat of reaction for the three kinds of samples are 3330, 1951, and 3494 J/g, respectively. There is no characteristic endothermic peak of Mg (melting point of bulk Mg is 650 °C) in both the DSC and DTA-TG curves, indicating that Mg has been totally consumed and the thermite reaction completes before the Mg melts. Typically, two (or more) exotherms appeared in the previously studied Al-based thermite reactions with a characteristic melting endothermic peak of Al (melting point of bulk Mg is 660 °C) between them,[21,23−25] even in the case of Al-lean compositions.[24,25] One possible reason for this is the nonuniform mixing of the fuel and oxidizer, leading to an incomplete reaction in a relatively low-heating temperature range.[22] There are also a few similar results for one exotherm reported with nanometric multilayered Al/CuO[5] and CuO nanowires/Al.[22] A nanometric multilayer can achieve uniform mixing, but serious premixing decreases the amount of heat release to a low value of 1200 J/g.[5] The sputtering technique was also adopted to deposit the shell layer,[22] which may contribute to the uniform mixing realized; however, the heat of reaction value was not given, and it should be somewhat low according to the small heat-flow values in the DSC trace. Nanoscale intimate contact and uniform mixing of Mg/CuO nanoenergetic arrays are both demonstrated in this work, and the amount of heat released (3300−3500 J/g) is very high compared with the previously reported values of 1800 J/g for an Al/MoO_3 nanoparticle composite,[4] 1200 J/g for a nanomultilayer Al/CuO,[5] 2500 J/g for CuO/Cu_2O nanowires/microfilm with Al,[24] and 2950 J/g for a similar structure.[21] Furthermore, the heat of reaction can be readily adjusted by changing the CuO deposition thickness to meet different requirements.

More importantly, sample 2 shows a large decrease in the heat of reaction (about 41%) compared with sample 1, which again proves that metallic nanostructures are easily oxidized and that protection is indispensable. However, sample 3 exhibits a comparable heat of reaction to that of sample 1, which successfully validates the long-term storage stability of our new Mg/CuO nanoenergetic arrays. We also note the heat of reaction of sample 3 is even slightly higher than that of sample 1 (but the difference is less than 5%), which is because of the small variation between each batch of the fabricated Mg nanorods.

Figure 7 shows typical SEM images of the reaction products of the Mg/CuO nanoenergetic arrays after the DSC test. The

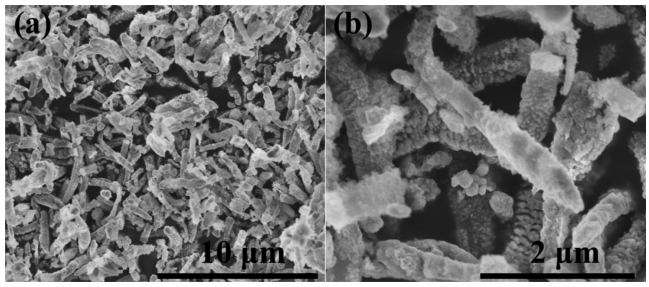

Figure 7. SEM images of the Mg/CuO nanoenergetic arrays after the DSC test. (a) Low magnification and (b) high magnification.

information provided by the images corresponds well with that of the DSC curve. The reaction products maintain their original rodlike morphology after the thermite reaction in DSC in Figure 6. The solid−solid reaction between Mg and CuO leads to the preserved rodlike morphology. The Mg nanorods are totally consumed before melting; otherwise, the remaining Mg nanorods will melt to form spheres because of the surface tension. Although the adiabatic temperature of the thermite reaction between Mg and CuO is very high (~2570 °C, which is well above the melting points of the reactants or products), DSC is a slow-heating characterization, which efficiently limits the self-heating of the samples. However, the combustion products (e.g., in open air) may exhibit different morphologies.

4. CONCLUSIONS

In this work, new core/shell nanoenergetic arrays are fabricated onto silicon substrates, with active Mg nanorods as the core and stable CuO as the shell. The synthesis method is facile and green, and it does not use a high-temperature treatment or chemical solution. Intimate contact and uniform mixing between the Mg fuel and CuO oxidizer are well realized. The Mg/CuO nanoenergetic arrays exhibit a superior heat-release property and long-term storage stability, which is very important for their practical applications (e.g., guaranteeing the reliability of a firing system). The results indicate that this new material can be an excellent candidate for various applications related to nanoenergetic materials, especially when long-term storage is needed. The concept adopted here may also be applied to other metals (e.g., Al) and metal oxides (e.g., Fe_2O_3, Co_3O_4, and MnO_2) to achieve different promising high-exothermic nanoenergetic arrays with long-term storage stability. Further work will be focused on the optimization of the energy release as well as practical ignition/combustion tests.

AUTHOR INFORMATION

Corresponding Author

*E-mail: kaizhang@cityu.edu.hk, kaili_zhang@hotmail.com.

Notes

The authors declare no competing financial interest.

ACKNOWLEDGMENTS

This work was supported by a grant from the Hong Kong Research Grants Council (project no. CityU 125412) and a contract research with the Institute of Chemical Materials at China Academy of Engineering Physics (contract no. XZ0862013002).

REFERENCES

(1) Bockmon, B. S.; Pantoya, M. L.; Son, S. F.; Asay, B. W.; Mang, J. T. *J. Appl. Phys.* **2005**, *98*, 064903-1−064903-7.
(2) Apperson, S.; Shende, R. V.; Subramanian, S.; Tappmeyer, D.; Gangopadhyay, S.; Chen, Z.; Gangopadhyay, K.; Redner, P.; Nicholich, S.; Kapoor, D. *Appl. Phys. Lett.* **2007**, *91*, 243109-1−243109-3.
(3) Son, S. F.; Asay, B. W.; Foley, T. J.; Yetter, R. A.; Wu, M. H.; Risha, G. A. *J. Propul. Power* **2007**, *23*, 715−721.
(4) Pantoya, M.; Granier, J. *Propellants, Explos., Pyrotech.* **2005**, *30*, 53−62.
(5) Petrantoni, M.; Rossi, C.; Salvagnac, L.; Conédéra, V.; Estève, A.; Tenailleau, C.; Alphonse, P.; Chabal, Y. J. *J. Appl. Phys.* **2010**, *108*, 084323-1−084323-5.
(6) Granier, J. J.; Pantoya, M. L. *Combust. Flame* **2004**, *138*, 373−383.
(7) Hunt, E. M.; Pantoya, M. L. *J. Appl. Phys.* **2005**, *98*, 034909-1−034909-8.
(8) Currano, L. J.; Churaman, W. A. *J. Microelectromech. Syst.* **2009**, *18*, 799−807.
(9) Zhang, K.; Rossi, C.; Petrantoni, M.; Mauran, N. *J. Microelectromech. Syst.* **2008**, *17*, 832−836.
(10) Korampally, M.; Apperson, S. J.; Staley, C. S.; Castorena, J. A.; Thiruvengadathan, R.; Gangopadhyay, K.; Mohan, R. R.; Ghosh, A.; Polo-Parada, L.; Gangopadhyay, S. *Sens. Actuators, B* **2012**, *171−172*, 1292−1296.
(11) Pantoya, M. L.; Hunt, E. M. *Appl. Phys. Lett.* **2009**, *95*, 253101-1−253101-3.
(12) Tillotson, T. M.; Gash, A. E.; Simpson, R. L.; Hrubesh, L. W.; Jr, J. H. S.; Poco, J. F. J. *Non-Cryst. Solids* **2001**, *285*, 338−345.
(13) Prakash, A.; McCormick, A. V; Zachariah, M. R. *Nano Lett.* **2005**, *5*, 1357−1360.
(14) Blobaum, K. J.; Reiss, M. E.; Plitzko, J. M.; Weihs, T. P. *J. Appl. Phys.* **2003**, *94*, 2915−2922.
(15) Umbrajkar, S. M.; Schoenitz, M.; Dreizin, E. L. *Thermochim. Acta* **2006**, *451*, 34−43.
(16) Schoenitz, M.; Umbrajkar, S. M.; Dreizin, E. L. *J. Propul. Power* **2007**, *23*, 683−687.
(17) Wang, S.; Shen, R.; Ye, Y.; Hu, Y. *Nanotechnology* **2012**, *23*, 435701.
(18) Dreizin, E. L. *Prog. Energy Combust. Sci.* **2009**, *35*, 141−167.
(19) Rossi, C.; Zhang, K.; Estève, D.; Alphonse, P.; Tailhades, P.; Vahlas, C. J. *J. Microelectromech. Syst.* **2007**, *16*, 919−931.
(20) Zhang, K.; Rossi, C.; Tenailleau, C.; Alphonse, P.; Chane-Ching, J.-Y. *Nanotechnology* **2007**, *18*, 275607.
(21) Zhang, K.; Rossi, C.; Ardila Rodriguez, G. A.; Tenailleau, C.; Alphonse, P. *Appl. Phys. Lett.* **2007**, *91*, 113117-1−113117-3.
(22) Ohkura, Y.; Liu, S.-Y.; Rao, P. M.; Zheng, X. *Proc. Combust. Inst.* **2011**, *33*, 1909−1915.
(23) Yang, Y.; Xu, D.; Zhang, K. *J. Mater. Sci.* **2011**, *47*, 1296−1305.
(24) Petrantoni, M.; Rossi, C.; Conédéra, V.; Bourrier, D.; Alphonse, P.; Tenailleau, C. *J. Phys. Chem. Solids* **2010**, *71*, 80−83.
(25) Xu, D.; Yang, Y.; Cheng, H.; Li, Y. Y.; Zhang, K. *Combust. Flame* **2012**, *159*, 2202−2209.
(26) Yetter, R. A.; Risha, G. A.; Son, S. F. *Proc. Combust. Inst.* **2009**, *32*, 1819−1838.
(27) Zhang, K.; Rossi, C.; Tenailleau, C.; Alphonse, P. *Appl. Phys. Lett.* **2008**, *92*, 063123-1−063123-3.
(28) Robbie, K.; Brett, M. J.; Lakhtakia, A. *Nature* **1996**, *384*, 616.
(29) Kwon, J.; Ducéré, J. M.; Alphonse, P.; Bahrami, M.; Petrantoni, M.; Veyan, J.-F.; Tenailleau, C.; Estève, A.; Rossi, C.; Chabal, Y. J. *ACS Appl. Mater. Interfaces* **2013**, *5*, 605−613.